Carbohydrate Polymers 90 (2012) 1648–1655

Contents lists available at SciVerse ScienceDirect

Carbohydrate Polymers

journal homepage: www.elsevier.com/locate/carbpol

Chitosan matrix with three dimensionally ordered macroporous structure for nimodipine release

Yuling Xie, Yanli Liu, Yan Wang, Siling Wang, Tongying Jiang*

Department of Pharmaceutics, Shenyang Pharmaceutical University, Shenyang 110016, China

ARTICLE INFO

Article history:
Received 11 June 2012
Received in revised form 12 July 2012
Accepted 18 July 2012
Available online 25 July 2012

Keywords:
3DOM
Chitosan
Nanometer range
Release behavior

ABSTRACT

Three dimensionally ordered macroporous (3DOM) chitosan (3D-CS) matrix with interconnected pores in the nanometer range was developed as a drug carrier for the first time. 3D-CS was prepared using a template-assisted assembly and characterized by SEM, TGA, N_2 adsorption and FT-IR. As a model drug, nimodipine (NMDP) was incorporated into the pores of 3D-CS matrix. The solid state properties of NMDP-loaded samples were characterized by SEM, XRD, DSC and FT-IR. Dissolution studies showed that release behavior of the drug was markedly affected by the particle size of the matrix. With a relatively small matrix particle size, formulations of NMDP-3D-CS-0.5 and NMDP-3D-CS-1 exhibited rapid release patterns. However, on increasing the amount of carrier, release rate of the drug decreased. The pH-dependent slow-release characteristic of 3D-CS matrix delivery system was demonstrated by investigating the release behavior of NMDP at different pH values.

© 2012 Elsevier Ltd. All rights reserved.

1. Introduction

In recent decades, three dimensionally ordered macroporous (3DOM) materials with well-defined surfaces, interconnected porous structures, and precisely controlled pore sizes in sub-micrometer range have shown great potential in the field of biosensors, catalysis, and photonic crystals (Liu et al., 2010; Lytle, Yan, Ergang, Smyrl, & Stein, 2004; Su et al., 2005). The attractive features of 3DOM materials made them possible to be cultivated as a drug carrier. The highly accessible macroporous networks of 3DOM materials could reduce diffusion resistance and enhance mass transport. Hu, Zhi, Wang, Jiang, and Wang (2011) incorporated indomethacin nanoparticles into a 3DOM–silica matrix. The crystal size of drug nanoparticles was reduced greatly compared with the pure IMC crystals due to spatial restriction of the pores. Rapid release profiles were observed for the IMC nanoparticle formulations. The enhanced dissolution rate may be attributed to the decreased crystallinity of IMC, as well as the hydrophilic surface and the interconnected pore networks of the 3DOM silica. 3DOM materials are generally prepared by the colloidal crystal template method. However, most of the 3DOM materials reported to date are mainly inorganic oxides, synthetic polymer materials, carbon and semiconductor materials (Bartlett, Birkin, Ghanem, & Toh, 2001; Holland, Blanford, Do, & Stein, 1999; Zakhidov et al., 1998; Zhu, Cao, Tang, Yang, & Li, 2009). There have been few reports on 3DOM materials made of natural polymers like polysaccharide.

Chitosan, a derivative of chitin, is a copolymer of N-acetyl-D-glucosamine (GlcNAc) and D-glucosamine (GlcN) (Charernsriwilaiwat, Opanasopit, Rojanarata, Ngawhirunpat, & Supaphol, 2010). With a high molecular weight, chitosan shows low solubility in water and most organic solvents. However, as a weak base, chitosan is soluble in acidic medium with the protonated amine groups. Due to its excellent properties such as biocompatibility, biodegradability and non-toxicity (Rinaudo, 2006), chitosan has been widely used in drug delivery systems (Muzzarelli, 2009). Chitosan could not only enhance the dissolution and bioavailability of a number of poorly water-soluble drugs (Mura, Zerrouk, Mennini, Maestrelli, & Chemtob, 2003; Mutalik, Anju, Manoj, & Usha, 2008) but also control the release of drugs (Chandy & Sharma, 1992; Thanoo, Sunny, & Jayakrishnan, 1992). As a natural polycationic polymer, different ionization state of amino groups on chains endows chitosan pH responsiveness. For this reason, there are many studies on the applications of chitosan in pH-responsive drug delivery systems (Chen & Zhu, 2011; Park, You, Park, Haam, & Kim, 2001; Popat, Liu, Lu, & Qiao, 2012; Santos, Neto, Fonseca, & Pereira, 2008). Moreover, large quantities of amino and hydroxyl groups on the chitosan chains endow it good wetting and adsorption properties (Chang, Chen, & Jiao, 2008). Consequently, it is reasonable to expect that its porous structure might have a high adsorptive capacity and be suitable for utilization in the drug delivery. In this paper, we have tried to prepare 3DOM chitosan, and exploit it as a new matrix for drug loading.

* Corresponding author.
E-mail address: tongyingjiang@yahoo.com.cn (T. Jiang).

0144-8617/$ – see front matter © 2012 Elsevier Ltd. All rights reserved.
http://dx.doi.org/10.1016/j.carbpol.2012.07.045

Chitosan has good film-forming properties (Park et al., 2001; Santos et al., 2008). This is favorable to make 3DOM chitosan because the polymer layer can stick tightly on the surface of the sacrificing spheres. However, during the procedure of drying the polymer into the corresponding gel structures, severe shrinkage and deformation usually take place. In many cases, the addition of inorganic components can improve the mechanical and thermal stability of the polymer matrix (Ayers & Hunt, 2001; Kierys, Dziadosz, & Goworek, 2010; Rashidova et al., 2004). And among so many solid powders, silica is a promising candidate for its excellent biocompatibility, stability and especially the miscibility with chitosan (Al-Sagheer & Muslim, 2010). So incorporation with silica may improve the structural strength of polymer matrix and effectively protect the chitosan matrix from deformation.

In the present study, 3DOM chitosan matrix with interconnected pore networks in the nanometer range was prepared using a template-assisted assembly. Nimodipine (NMDP), a poorly water-soluble drug was incorporated into the pores of the matrix and the effects of drug loading and the matrix particle size on the release behavior of NMDP was evaluated. In addition, dissolutions at different pH values were investigated to explore the nature of pH-dependent release of our matrix delivery system.

2. Experimental

2.1. Materials

Styrene, tetrahydrofuran, glacial acetic acid, methanol, and tetraethyl orthosilicate (TEOS) were obtained from Aladdin (Shanghai, China). Nimodipine was supplied from Zhejiang Wenzhou Qingming Chemical Industry (China). Chitosan (degree of deacetylation 95%, M_w 13.44×10^4) were purchased from Yuhuan Ocean Biochemistry Co. Ltd. (Zhejiang, China). All chemicals were analytical grade and used as purchased without further purification. Deionized water was prepared by ion exchange.

2.2. Preparation of 3DOM chitosan (3D-CS)

Polystyrene (PS) microspheres were synthesized by soap-free emulsion polymerization (Zhang et al., 2009). The PS particles were rinsed once using 0.5%SDS aqueous solution, and then re-dispersed in pure water. The well organized colloidal crystal was self-assembled by evaporating the water at the temperature of 50 °C (Fu, Jin, Liu, & Yin, 2009). The well-ordered PS templates were strengthened by annealing at 80 °C for 1 h.

Chitosan (1.0 g) was dissolved in 200 ml of aqueous 5 wt% acetic acid to form a transparent solution (0.5%, w/v). The precursor of silica alkoxide was made by adding 5 ml HCl (0.5 M) in 24 ml deionized water and then mixing with 15 ml TEOS. The mixtures were stirred with a magnetic stirrer for 15 min, and used until the precursor cooled to room temperature. The colloidal crystal templates were incubated in the chitosan solution for 30 min which was removed by vacuum filtration afterwards. The deposition progress was repeated once. Then the composite was soaked into the silica precursor and the immersion procedure lasted for 15 min. The obtained compound was treated by chitosan solution once more. All the drying temperature was 60 °C after the infusion process. The template spheres were removed using tetrahydrofuran, until no PS remained which was evaluated by DSC.

For comparison, silica with 3DOM structure was prepared by filling of the interstice of the template with silica alkoxide.

2.3. Drug loading procedures

NMDP nanoparticles were incorporated into the pores of 3D-CS matrix by immersion and solvent evaporation. Before the loading process, the obtained 3D-CS solid monolith was crushed gently for a few minutes, and then passed through 60-mesh and 160-mesh sieves to obtain matrixes with large and relatively small particle size range, respectively. Specific quality of 3D-CS matrixes (mass ratios of NMDP and carrier were 1/0.5, 1/1 and 1/2, w/w) was immersed in a methanol solution of NMDP (50 mg/ml). After the suspension was stirring gently for 6 h in a sealed container, the solvent was permitted to evaporate at ambient temperature during the stirring. For different mass ratios of the drug and carrier, preparations were labeled as NMDP-3D-CS-0.5, NMDP-3D-CS-1, and NMDP-3D-CS-2.

2.4. Drug content analysis

Specific amount of NMDP-loaded preparations were suspended in 100 ml ethanol. Then the mixture was ultrasonicated to extract the drug completely. Drug concentration was detected by UV-VIS spectrophotometry (UV-2000, Unico, USA) at a wavelength of 238 nm. Three replicates were done for every sample analysis.

2.5. SEM characterization

The morphology of samples was characterized using a field emission scanning electron microscopy (JSM-6301F, JEOL, Japan). Prior to imaging, a small quantity of the samples were fixed on the metal stubs and sputtered with gold under vacuum.

2.6. Thermal analysis of 3D-CS

The thermal behaviors of the 3D-CS and 3D-silica were characterized using a TGA-50 instrument (Shimadzu, Japan). Samples about 3 mg was heated at a rate of 10 °C/min under a nitrogen flow of 40 ml/min.

2.7. Nitrogen adsorption analysis

Surface area of the 3D-CS and drug-loaded samples was studied using a surface area analyzer (SA3100, Beckman Coulter, USA) at −196 °C. 3D-CS matrix was degassed at 80 °C for 3 h, and nimodipine-loaded preparations were degassed at 50 °C for 3 h. The surface area was determined according to the Brunauer–Emmett–Teller (BET) from the adsorption branches of the isotherms.

2.8. XRD and DSC studies

The physical state of the samples was examined on a differential scanning calorimeter (DSC 60, Shimadzu Co., Japan). The accurately weighted samples were loaded in pierced aluminum pans. The measurements were conducted from 50 °C to 140 °C with a heating scan of 10 °C/min under a nitrogen purge of 40 ml/min.

XRD patterns of the samples were collected using a Rigaku Geigerflex powder X-ray diffractometer (Rigaku Denki, Japan) with a copper anode (Cu Kα radiation, λ = 0.15405 nm, 30 kV, 30 mA). XRD patterns were recorded over the 2θ angle range from 5° to 45° with a step size of 0.03° and a scan speed of 4°/min. The XRD date analysis software-MDI Jade 5.0 was used to calculate percent crystallinity and crystallite size of pure drug and drug-loaded samples.

2.9. FT-IR characterization

FT-IR spectra of the samples were examined on a FT-IR spectrometer (Bruker IFS 55, Switzerland) using KBr pellet technique. The samples were milled to a fine powder and mixed with dried KBr

(mass ratio of samples and KBr was about 1–2:100) in an agate mortar and pestle. The KBr pellet was made in a 13 mm diameter round flat face punch. The IR spectra were collected over the spectroscopic range from 400 to 4000 cm^{-1}, in a transmittance mode.

2.10. In vitro dissolution

In vitro drug release was evaluated in phosphate buffer solution (pH 6.8) with 0.3% SLS (w/v). Dissolution experiments were carried out using a USP II paddle method (75 rpm, 37 °C and 900 ml dissolution medium) on a D-800LS dissolution tester (Tianjin University Radio Factory, China). NMDP-loaded samples equivalent to 20 mg NMDP were added to the dissolution juice at zero time. 5 ml aliquots of the release medium were withdrawn and passed through a 0.22 μm membrane filter at predetermined intervals. And then the concentration of the released NMDP was detected at wavelength of 238 nm by UV–VIS spectrophotometry. All measurements were conducted in triplicate. In vitro dissolution was also performed in pH 1.2 (HCl aqueous solution) and pH 4.5 (prepared using NaAc and HAc) solutions containing 0.3% SLS (w/v).

2.11. Relationship between pH and drug release

To investigate the state of chitosan in solutions at different pH values, samples with the same weight were taken into pH 1.2, pH 4.5 and pH 6.8 solutions. The mixtures were shaking in an air bath maintained at 37 °C. Water sorption capacity of 3D-CS in fluid at different pH values was also examined. At predetermined time intervals of 0.25 h, 0.5 h, 1 h, 1.5 h, 2 h, 3 h, fluids were remove, and the excess water was blotted from surface of the samples with filter papers. The water adsorption (W%) was calculated according to

$$W(\%) = \frac{m_s - m}{m} \times 100$$

where m_s presents the mass of wet samples, and m is the mass of samples before water uptake.

3. Results and discussion

3.1. Preparation and morphology of the 3D-CS matrix

The 3D-CS matrix was synthesized by the colloidal crystal template method (Xia, Gates, Yin, & Lu, 2000). In the present

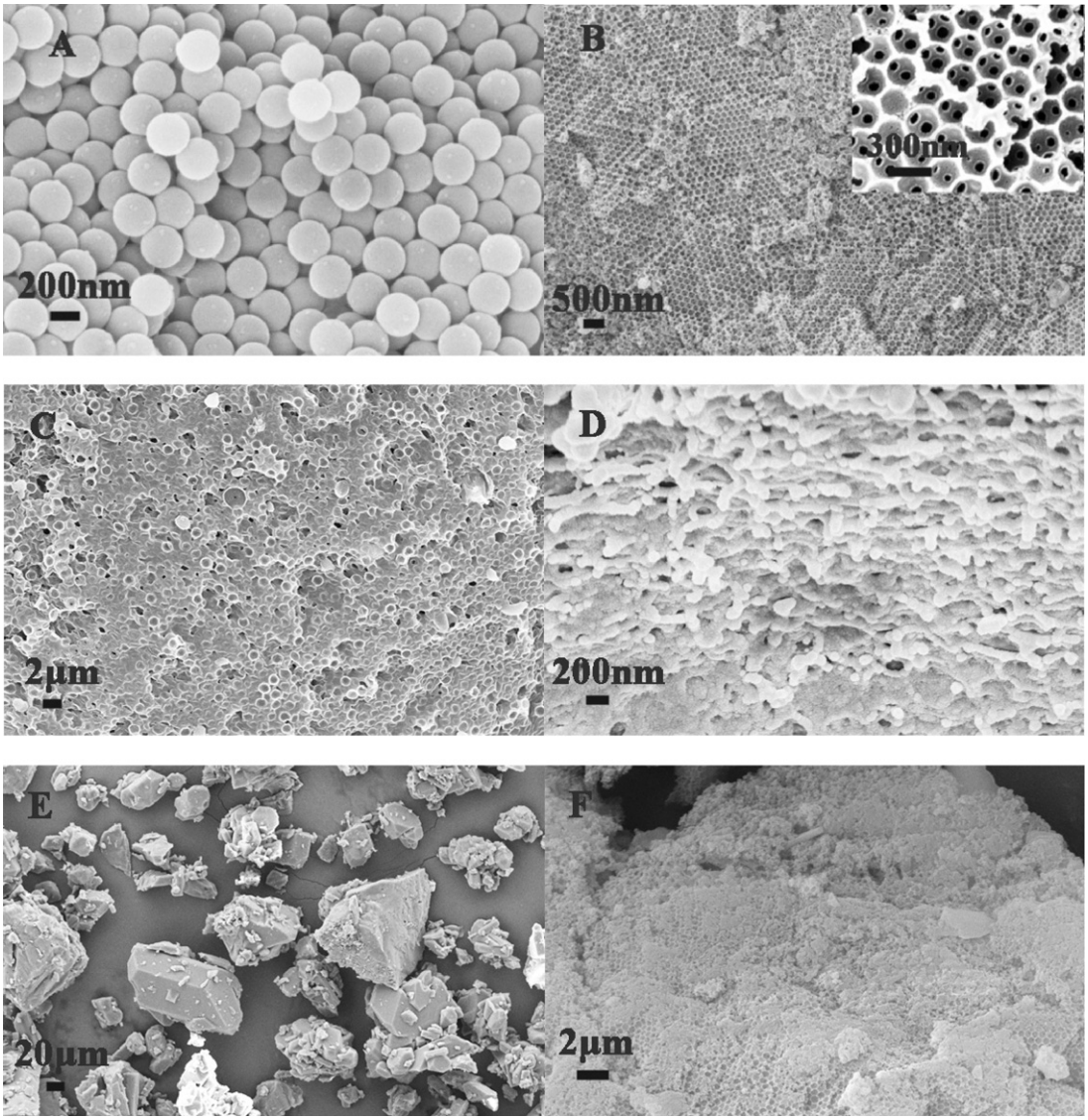

Fig. 1. SEM images of PS microspheres (A), 3D-CS matrix (B), chitosan membrane without combination with silica top surface (C), cross-section (D), pure NMDP (E) and NMDP-loaded samples (F).

experiment, PS latex spheres were prepared by soap-free emulsion polymerization and organized as the colloidal crystal template. The spheres were washed with SLS solution for two reasons. The first reason was the surfaces of the PS nanospheres are hydrophobic; to the contrary, the chitosan solution was hydrophilic. The procedure of treating with SLS solution created hydrophilic surfaces for the colloidal particles, which made the recombination process more efficient. The second reason was because when anionic surfactants are absorbed on the surface of the spheres, positively charged chitosan is deposited on the surface of PS particles compactly due to electrostatic interaction. Therefore, a flat and rigid layer of chitosan is formed (Dedinaite & Ernstsson, 2003), which could be seen from SEM images of 3D-CS (Fig. 1B). During the preparation process, layer by layer fusion (Cai, Rechtenbach, Hao, Bossert, & Jandt, 2005; Caruso, Trau, Möhwald, & Renneberg, 2000) was used with the sol–gel technique (Lai, Yang, & Chen, 2006). Only the chitosan membrane was obtained without silica incorporation owing to polymer shrinkage and deformation, as shown in Fig. 1C and D. The combination of the inorganic phase significantly improved the mechanical stability of the polymer matrix successfully. As shown in Fig. 1A, the diameter of PS spheres was about 280 nm, with a narrow size distribution. The 3D-CS matrix exhibited ordered and interconnected macroporous structure. In addition, diameter of the spherical pores was about 180 nm and the circular windows between pores was about 50 nm (Fig. 1B). Thus it can be seen that the size of spherical pores was decreased as compared to the size of PS spheres. This may be due to the process of template annealing, and the shrinkage after template sacrificing. It was a facile method to prepare the 3D-CS matrix with specific pore size in the nanometer range. And pore size of the matrix could be tailored by the spheres size. It was believed that 3D-CS with the unique structure should have advantages on drug delivery.

3.2. Morphology of pure NMDP and NMDP-loaded samples

As shown in Fig. 1E, pure NMDP was irregularly shaped with a wide particle size distribution of dozens of micrometers. After inclusion of the drug into the pores of the polymer matrix, large drug particles disappeared and the macropores on the surface were blocked leaving only traces of pore arrays (Fig. 1F), which was fit with the decreasing specific surface area of the drug-loaded samples.

3.3. TGA analysis of 3D-CS

As shown in Fig. 2, TGA was detected over the range of 20–580 °C. Silica exhibited no obvious weight loss within this temperature range. In the case of 3D-CS, the initial weight loss observed between

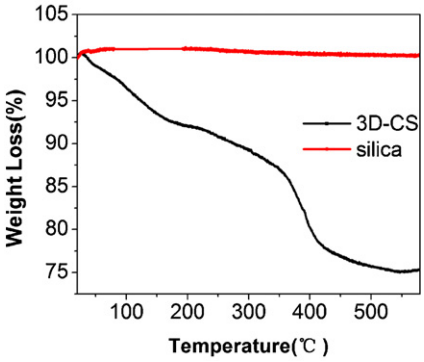

Fig. 2. TGA for 3D-CS and 3D-silica.

40 °C and 200 °C appears to be the loss of absorbed water on the chitosan surface. Chitosan exhibited a weight loss between 200 °C and 530 °C. The slower weight loss in the region between 200 °C and 350 °C was due to the decomposition of low molecular weight species of chitosan. Thermal decomposition was more marked in the region between 350 °C and 530 °C relating to the complex dehydration of the saccharide rings, depolymerization, and decomposition of the acetylated and deacetylated polymer units (Peniche-Covas, Argüelles-Monal, & San Román, 1993). As calculated from the TGA graph, the total weight loss for chitosan was about 16.5%.

3.4. Estimation of the specific surface area from N_2 adsorption

As shown in Table 1, 3D-CS had a large surface area calculated to be 102.8 m^2/g. After introduction of NMDP, the specific surface area of the samples decreased markedly compared with the 3D-CS matrix. As the drug content increased, the specific surface area of samples tended to decrease. Both showed that NMDP nanoparticles were incorporated into the pores of the 3D-CS matrix efficiently.

Table 1
Specific surface area and drug loading of samples before and after NMDP uptake.

Samples	S_{BET} (m^2/g)	Drug loading
3D-CS	102.8	–
NMDP-3D-CS-0.5	11.9	65.4–73.3%
NMDP-3D-CS-1	29.6	47.5–51.2%
NMDP-3D-CS-2	30.7	31.2–33.7%

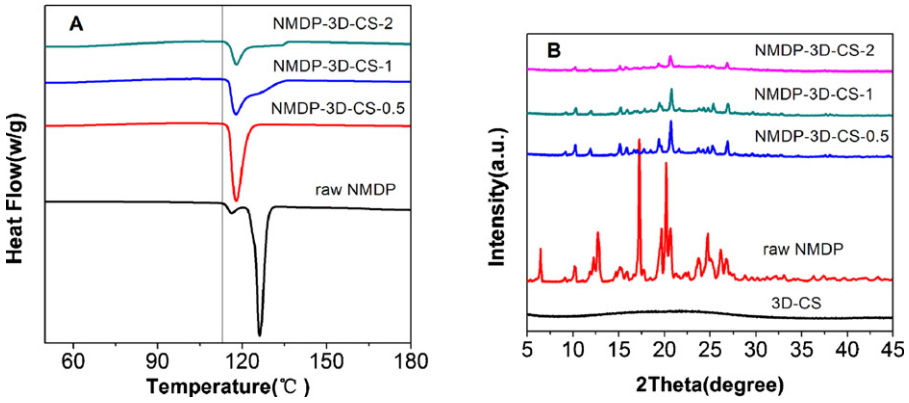

Fig. 3. DSC (A) and XRD (B) patterns for 3D-CS, pure NMDP and NMDP-loaded samples.

3.5. DSC and XRD evaluation of crystallinity

As shown in Fig. 3, pure NMDP reflected two crystal modifications: mod I (124 ± 1 °C) and mod II (114 ± 1 °C), which agreed with literature reports (Grunenberg, Keil, & Henck, 1995; Guo et al., 2011). NMDP-loaded samples with a different mass ratio (NMDP/3D-CS 1/0.5, 1/1, 1/2) all showed crystal form of mod II. In the case of NMDP-3D-CS-1 and NMDP-3D-CS-2, the shoulder following the main peak was probably related to the amorphism of the drug. This was reasonable. NMDP was inclined to crystal as form II in the presence of solvent (e.g., isopropanol and ethanol) (Grunenberg et al., 1995). Also, mod II is the thermodynamically stable form of the drug.

The XRD patterns of pure NMDP and NMDP-loaded samples are shown in Fig. 3. All the results were in accordance with the DSC profiles. In the diffraction patterns of pure NMDP, the characteristic peaks $2\theta = 6.7^\circ$ and $2\theta = 10.40^\circ$ for mod I and mod II, respectively were observed. Peak $2\theta = 10.4^\circ$ was presented in NMDP-loaded samples, implying the crystal form of mod II. The intensity was reduced markedly compared with pure NMDP. Also, the intensity of the preparations decreased as the amount of carrier increased. Moreover, the crystal size of pure NMDP was about 29 nm calculated by Jade 5.0 software. Changes in grain size were evident in preparations, namely, 12 nm, 11 nm, and 9 nm for NMDP-3D-CS-0.5, NMDP-3D-CS-1, and NMDP-3D-CS-2, respectively. The drug crystal size was reduced greatly after incorporation into the chitosan matrix compared with pure NMDP. This may be because aggregation and crystal growth of the drug were prevented when the drug nanoparticles were fixed in the pores of the matrix. In addition, on increasing the mass proportion of 3D-CS, the chances of aggregation and crystal growth of the drug were reduced thereby the drug crystal size was also decreased. Besides, hydrogen bonding lying between drug and the carrier may make contributions to the observed loss of crystallinity (Madieh, Simone, Wilson, Mehra, & Augsburger, 2007).

3.6. FT-IR characterization

Fourier transform infrared (FT-IR) spectra were recorded to illustrate the interfacial interaction between the inorganic phase and the polymer (Fig. 4A). The characteristic absorbance of 3D-CS shows the stretching vibration of C=O at 1635 cm^{-1} and the bending due to Amide II at 1384 cm^{-1} (Al-Sagheer & Muslim, 2010; Lei & Bi, 2007). The C—O skeletal stretching was observed at 1098 cm^{-1}. A broad band that appeared at 3430 cm^{-1} is due to the amine N—H symmetric stretching vibration. In contrast, the N—H vibration is observed at 3435 cm^{-1} for the simple physical mixture of silica and chitosan. The peak shifted to a slightly lower frequency in the N—H regions after in situ incorporation of silica (Al-Sagheer & Muslim, 2010), suggesting the increased interfacial interaction between chitosan and the inorganic phase. The appearance of the new absorption band at 957 cm^{-1} involved the Si—OH bonds (Lai et al., 2006) which is due to the formation of hydrogen bonds between the silanol groups of the silica network and the amide or oxy-groups of chitosan (Rashidova et al., 2004). Specific bands in the region of 1000–1250 cm^{-1} belonging to the characteristic absorption of Si—O—Si are clearly observed in the modified system.

The FT-IR spectra of NMDP, 3D-CS, the physical mixture and NMDP-3D-CS are shown in Fig. 4B. Crystalline form of pure NMDP was indicated from the N—H stretch at 3299 cm^{-1}. The carbonyl peak at 1700 cm^{-1} indicated their non-hydrogen bonded status (Tang, Pikal, & Taylor, 2002). The absorbance of $-NO_2$ group at 1523 cm^{-1}, the C=C stretching at 1640 cm^{-1} and the aromatic C=C stretches at 1620 cm^{-1} were showed in the IR spectra of pure NMDP (Papadimitriou, Papageorgiou, Kanaze, Georgarakis, & Bikiaris, 2009). The characteristic peaks of the drug were also obvious in the FT-IR spectra of NMDP-3D-CS. It was verified that NMDP was entrapped into the polymer matrix. On the other hand, the peak at 1696 cm^{-1} and 1674 cm^{-1} of the drug-loaded samples, somewhat indicated amorphous state of the drug and the decreasing hydrogen bond strength between drug molecular (Tang et al., 2002). Besides, the shift and weakening of the N—H stretching vibration (3271 cm^{-1}) proved hydrogen bonding between the drug and polymer as well as (Zheng, Yang, Tang, & Zheng, 2007). Besides, except for the absorbance at 3271 cm^{-1}, typical features of NMDP-loaded sample showed no new peaks and shift of the characteristic peak position compared with the physical mixture, indicating the physical adsorption of NMDP in the 3D-CS as well. For the porous materials-based drug delivery systems, physical adsorption commonly exists between the drug and the carrier (Wu et al., 2011; Zhao et al., 2011).

3.7. In vitro dissolution studies

In this present work, the effect of polymer matrix particle size on drug release was investigated. The release patterns of NMDP nanoparticles preparations with different drug loadings were measured and compared with crude drug. As shown in Fig. 5B, rapid releases were displayed for NMDP-3D-CS-0.5 and NMDP-3D-CS-1 above 90% and nearly 80%, respectively after 1 h. Both of the nanoparticles formulations were prepared using 3D-CS matrix with a small mean particle size. By contrast, cumulative release of the crude drug was only 30%. Several factors may make contributions to the dissolution enhancement. Reduction of drug crystal size to the nanometer range due to space restriction could increase dissolution velocity effectively according to the Noyes–Whitney and

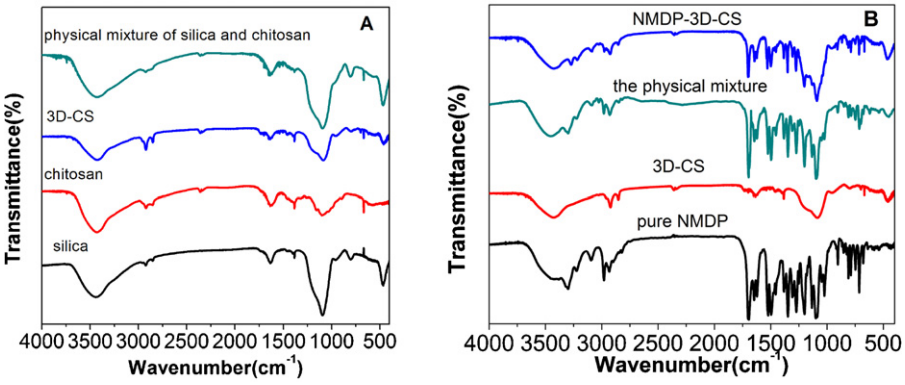

Fig. 4. FT-IR spectra for pure chitosan, silica, the physical mixture and 3D-CS (A) 3D-CS, pure NMDP, the physical mixture and NMDP-loaded samples (B).

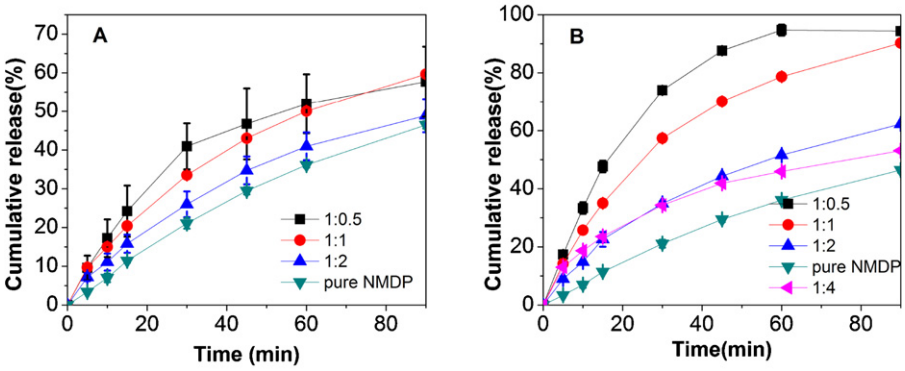

Fig. 5. Dissolution profiles of drug-loaded samples having a large particle size range (A) and a relatively small particle size range (B) with different mass ratios of NMDP/3D-CS 1/0.5, 1/1, 1/2, 1/4.

Ostwald–Freundlich equation (Kesisoglou, Panmai, &Wu, 2007). And the formation of less ordered crystals as drug nanoparticles were confined in the lattice of the matrix is well known to increase solubility and dissolution rate of poorly water-soluble drugs. The wetting properties of chitosan might also make a contribution. Moreover, interconnected pore networks of the 3DOM matrix could ease transport of poorly water-soluble drugs and enhance drug dissolution. However, the cumulative release of NMDP-3D-CS-2 was only 50% in 1 h. On increasing the mass ratio of NMDP: 3D-CS up to 1:4, there was no obvious improvement in drug release. So a higher drug loading was preferred for our drug delivery system. This was consistent with a number of published reports. Bayomi, AL-Suwayeh, El-Helw, and Mesnad (1998) found that the release of drug from chitosan hydrogels increased with an increasing drug content in the matrix systems. By comparison, drug-loaded samples using matrix with a large mean particle size exhibited a 65% maximum release after 2 h (Fig. 5A). It appeared that the dissolution rate decreased as the weight ratio of 3D-CS matrix increased as well as. From the order of release rate for preparations using 3D-CS matrix with both large and small particle sizes, the sustained-release properties of the polymer matrix were revealed. When the drug-loaded samples were immersed into the release medium at pH 6.8, chitosan layer of the matrix became hydrated and existed in the form of a gel network (Chen & Zhu, 2011). This may hinder the release of NMDP, nevertheless, it did not block pores completely allowing drug diffusion. Considering the rapid release of NMDP-3D-CS-0.5 and NMDP-3D-CS-1, the reduction of drug nanoparticles might play an important role. More importantly, the greater concentration gradient of the drug might be the driving force to diffuse through the swelling porous structure to reach the release medium. The comparison between the drug release behaviors for preparations using matrix with different mean particle size suggested that the length of diffusion pathway made significance on drug release. In the case of samples with relatively small particle size, more drug particles dispersed on the surface and outside pores of the chitosan matrix. Drug released rapidly when the preparations were soaked in the solution, since the solvent penetrated into the matrix pores quickly. Delayed release patterns were shown for samples with large particle size. This suggests that NMDP is released mainly by diffusion. According to Fick's law, the diffusion rate decreases as the mean length of the diffusion pathway increases (Heng, Chan, Easterbrook, & Li, 2001).

3.8. Investigation of relationship between pH and drug release

From the water adsorption for chitosan, it was found that chitosan swelled to gel and underwent rapid erosion in solution at pH 1.2. The water adsorption in solution at pH 6.8 was markedly higher than at pH 4.5 (Fig. 6A). At higher pH condition, the chitosan network is loose with a greater hydrodynamic free volume and availability of hydrophilic groups for the water to form hydrogen bonds, so that the chains can suck up more water resulting in higher swelling (Soppimath, Kulkarni, & Aminabhavi, 2001). At pH 4.5, the formation of the gel layer decreases the extent of polymer chain relaxation which hindered water adsorption. By comparison, the water adsorption of 3D-CS was clearly lower than that of the pure chitosan (Fig. 6B). This implied that chitosan chains were partially bound by polysiloxane network after incorporation of silica in the interstice. The different release patterns of the drug in different pH media were mainly due to different swelling states and water adsorption of the chitosan layer, as well as the drug distribution. When the 3D-CS matrix was immersed in pH 1.2 solution, the channel wall of chitosan layer became viscous, which will certainly

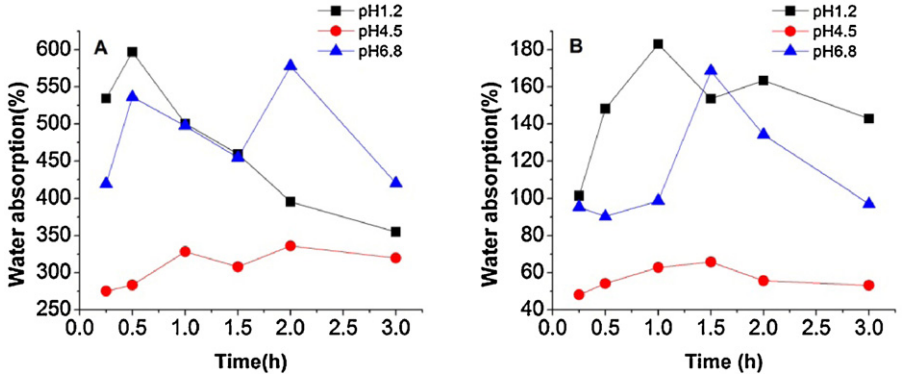

Fig. 6. Water adsorption of pure chitosan (A) and 3D-CS (B).

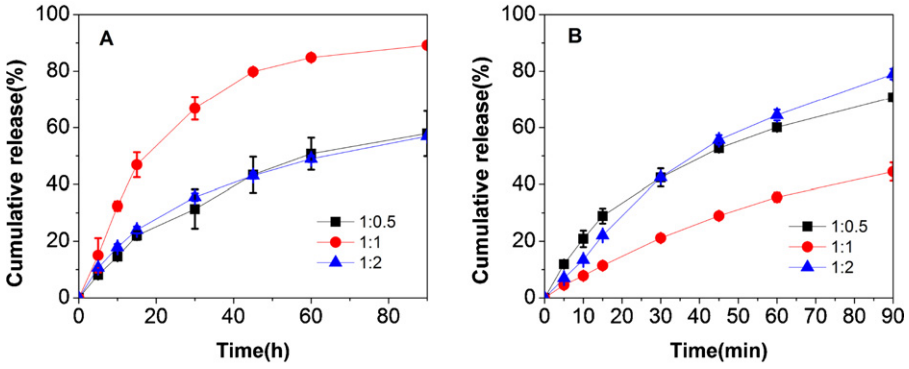

Fig. 7. Dissolution profiles of drug-loaded samples at intermedium pH 4.5 (A) and pH 1.2 (B) with different mass ratios of NMDP/3D-CS 1/0.5, 1/1, 1/2.

Table 2
Results for fitting NMDP release data to different kinetic equations in media at different pH values.

Media	Higuchi model K (R^2)	Korsmeyer–Peppas model n (R^2)	First order model K (R^2)	Zero order model K (R^2)
	0.013(0.980)	0.681(0.971)	0.049(0.998)	1.547(0.912)
pH	0.010(0.984)	0.582(0.979)	0.007(0.960)	0.887(0.907)
6.8	0.070(0.988)	0.676(0.989)	0.010(0.988)	0.623(0.947)
	0.058(0.992)	0.489(0.993)	0.007(0.960)	0.467(0.922)
	0.071(0.988)	0.009(0.971)	0.005(0.933)	0.685(0.983)
pH	0.104(0.918)	0.024(0.942)	0.008(0.798)	0.602(0.920)
4.5	0.640(0.989)	0.008(0.968)	0.005(0.924)	0.579(0.985)
	0.081(0.991)	0.012(0.987)	0.006(0.930)	0.611(0.984)
pH	0.057(0.996)	0.006(0.991)	0.004(0.973)	0.809(0.996)
1.2	0.104(0.993)	0.017(0.998)	0.008(0.944)	0.860(0.983)

Notes: Results at pH 6.8 are fittings for NMDP-3D-CS-0.5, NMDP-3D-CS-1, NMDP-3D-CS-2 and NMDP-3D-CS-4, respectively. The following results at pH 4.5 and pH 1.2 are fittings for NMDP-3D-CS-0.5, NMDP-3D-CS-1 and NMDP-3D-CS-2, respectively.

hindered diffusion of the drug. As shown in Fig. 7B, cumulative release of the drug was only 50% after 1 h. The release in pH 4.5 solution was also low except for the rapid release of NMDP-3D-CS-1 (Fig. 7A). Water adsorption of chitosan matrix in solution at pH 4.5, was slower and lower than at pH 6.8 owning to the higher gel formation acting as a barrier in the lower pH medium (Huanbutta et al., 2011). And the disparity of dissolution between the samples with different drug loadings may be ascribed to the drug distribution. With high drug loading of NMDP-3D-CS-0.5, the presence of crystal form located on the surface and lower water adsorption of chitosan at pH 4.5 leaded to slow release of the drug. The rate and amount of water uptake affected drug release (Soppimath et al., 2001). In the case of NMDP-3D-CS-1, more drug particles within the pores of the matrix created crowded channel which prevented gel formation of the chitosan layer, resulting in a rapid release. At low drug loading about 31–33%, most drug nanoparticles of NMDP-3D-CS-2 were distributed deep inside of the macropores. The drug release may get more hindrances from the higher gel layer of chitosan. Besides, when the drug-loaded samples were immersed in the dissolution medium, concentration gradient of NMDP-3D-CS-2 was smaller than that of NMDP-3D-CS-1. So a slow release pattern was showed for NMDP-3D-CS-2 as well. The 3D-CS matrix adsorbed water more quickly before gel formation in pH 6.8 solution, and then the chitosan chains entangled in the gel state, both of that are good for the release of guest molecules (Chen & Zhu, 2011). This indicates that the higher ratio of gel formation, the lower drug dissolution. The drug release in solutions at different pH values suggested pH-dependent release of our new matrix delivery system. Fitting of the release data to different release kinetics (Table 2) indicates that NMDP released from 3D-CS matrix with small particle size in media at different pH values are Fickian diffusion and agreed well with Higuchi's model. The good fit obtained suggests that the release rate depends upon the rate of diffusion through the porous matrix (Agnihotri, Mallikarjuna, & Aminabhavi, 2004).

4. Conclusion

A novel 3D-CS matrix was prepared successfully using a template-assisted assembly. NMDP nanoparticles were encapsulated into the pores of 3D-CS matrix effectively and characterized by SEM, N_2 adsorption, XRD, DSC and IR. The hydrogen bonding existing between the guest molecule (drug) and 3D-CS host was observed. Moreover, a loss of crystallinity and the decreased crystal size of the drug were revealed. In addition, the drug-loaded samples showed reflections of mod II. In vitro dissolution studies showed that mean particle size of 3D-CS matrix affected drug release greatly. The drug released rapidly from the 3D-CS matrix only when the particle size of the matrix was relatively small. Moreover, the concentration gradient of the drug must great enough to diffuse across the porous structure of polymer matrix. So a high drug loading was preferred in our drug delivery system. From the investigations of the relationship between pH values of media and release behaviors of the drug, it was found that the higher ratio of gel formation, the lower the drug release rate, confirming the pH-dependent slow-release properties of our new matrix delivery system.

Acknowledgements

This work was supported by National Basic Research Program of China (973 Program) (No. 2009CB930300), National Natural

Science Foundation of China (No. 81072605), Major National Platform for Innovative Pharmaceuticals (2009ZX09301-012), Key Laboratory of Drug Preparation Design & Evaluation of Liaoning Provincial Education Department (LS2010161) and Shenyang Special Fund for Exploration of Intellectual Resources.

References

Agnihotri, S. A., Mallikarjuna, N. N., & Aminabhavi, T. M. (2004). Recent advances on chitosan-based micro-and nanoparticles in drug delivery. *Journal of Controlled Release*, *100*, 5–28.

Al-Sagheer, F., & Muslim, S. (2010). Thermal and mechanical properties of chitosan/SiO_2 hybrid composites. *Journal of Nanomaterials*, 7. Article ID: 490679.

Ayers, M. R., & Hunt, A. J. (2001). Synthesis and properties of chitosan–silica hybrid aerogels. *Journal of Non-Crystalline Solids*, *285*, 123–127.

Bartlett, P. N., Birkin, P. R., Ghanem, M. A., & Toh, C. S. (2001). Electrochemical syntheses of highly ordered macroporous conducting polymers grown around self-assembled colloidal templates. *Journal of Materials Chemistry*, *11*, 849–853.

Bayomi, M. A., A.L-Suwayeh, S. A., El-Helw, A. M., & Mesnad, A. F. (1998). Preparation of casein–chitosan microspheres containing diltiazem hydrochloride by an aqueous coacervation technique. *Pharmaceutica Acta Helvetiae*, *73*, 87–192.

Cai, K., Rechtenbach, A., Hao, J., Bossert, J., & Jandt, K. D. (2005). Polysaccharide-protein surface modification of titanium via a layer-by-layer technique: Characterization and cell behaviour aspects. *Biomaterials*, *26*, 5960–5971.

Caruso, F., Trau, D., Möhwald, H., & Renneberg, R. (2000). Enzyme encapsulation in layer-by-layer engineered polymer multilayer capsules. *Langmuir*, *16*, 1485–1488.

Chandy, T., & Sharma, C. P. (1992). Chitosan beads and granules for oral sustained delivery of nifedipine: In vitro studies. *Biomaterials*, *13*, 949–952.

Charernsriwilaiwat, N., Opanasopit, P., Rojanarata, T., Ngawhirunpat, T., & Supaphol, P. (2010). Preparation and characterization of chitosan-hydroxybenzotriazole/polyvinyl alcohol blend nanofibers by the electrospinning technique. *Carbohydrate Polymers*, *81*, 675–680.

Chen, F., & Zhu, Y. (2011). Chitosan enclosed mesoporous silica nanoparticles as drug nano-carriers: Sensitive response to the narrow pH range. *Microporous and Mesoporous Materials*, *150*, 83–89.

Dedinaite, A., & Ernstsson, M. (2003). Chitosan–SDS interactions at a solid–liquid interface: Effects of surfactant concentration and ionic strength. *The Journal of Physical Chemistry B*, *107*, 8181–8188.

Fu, Y., Jin, Z., Liu, G., & Yin, Y. (2009). Self-assembly of polystyrene sphere colloidal crystals by in situ solvent evaporation method. *Synthetic Metals*, *159*, 1744–1750.

Grunenberg, A., Keil, B., & Henck, J. O. (1995). Polymorphism in binary mixtures, as exemplified by nimodipine. *International Journal of Pharmaceutics*, *118*, 11–21.

Guo, Z., Ma, M., Wang, T., Chang, D., Jiang, T., & Wang, S. (2011). A kinetic study of the polymorphic transformation of nimodipine and indomethacin during high shear granulation. *AAPS PharmSciTech*, *12*, 610–619.

Heng, P. W. S., Chan, L. W., Easterbrook, M. G., & Li, X. (2001). Investigation of the influence of mean HPMC particle size and number of polymer particles on the release of aspirin from swellable hydrophilic matrix tablets. *Journal of Controlled Release*, *76*, 39–49.

Holland, B. T., Blanford, C. F., Do, T., & Stein, A. (1999). Synthesis of highly ordered, three-dimensional, macroporous structures of amorphous or crystalline inorganic oxides, phosphates, and hybrid composites. *Chemistry of Materials*, *11*, 795–805.

Hu, Y., Zhi, Z., Wang, T., Jiang, T., & Wang, S. (2011). Incorporation of indomethacin nanoparticles into 3-D ordered macroporous silica for enhanced dissolution and reduced gastric irritancy. *European Journal of Pharmaceutics and Biopharmaceutics*, *79*, 544–551.

Huanbutta, K., Sriamornsak, P., Limmatvapirat, S., Luangtana-anan, M., Yoshihashi, Y., Yonemochi, E., et al. (2011). Swelling kinetics of spray-dried chitosan acetate assessed by magnetic resonance imaging and their relation to drug release kinetics of chitosan matrix tablets. *European Journal of Pharmaceutics and Biopharmaceutics*, *77*, 320–326.

Kesisoglou, F., Panmai, S., & Wu, Y. (2007). Nanosizing – Oral formulation development and biopharmaceutical evaluation. *Advanced Drug Delivery Reviews*, *59*, 631–644.

Kierys, A., Dziadosz, M., & Goworek, J. (2010). Polymer/silica composite of core–shell type by polymer swelling in TEOS. *Journal of Colloid and Interface Science*, *349*, 361–365.

Lai, S. M., Yang, A. J. M., & Chen, W. C. (2006). The properties and preparation of chitosan/silica hybrids using sol–gel process. *Polymer-Plastics Technology and Engineering*, *45*, 997–1003.

Lei, Z., & Bi, S. (2007). The silica-coated chitosan particle from a layer-by-layer approach for pectinase immobilization. *Enzyme and Microbial Technology*, *40*, 1442–1447.

Liu, J., Cai, Y., Deng, Y., Sun, Z., Gu, D., Tu, B., et al. (2010). Magnetic 3-D ordered macroporous silica templated from binary colloidal crystals and its application for effective removal of microcystin. *Microporous and Mesoporous Materials*, *130*, 26–31.

Lytle, J. C., Yan, H., Ergang, N. S., Smyrl, W. H., & Stein, A. (2004). Structural and electrochemical properties of three-dimensionally ordered macroporous tin (IV) oxide films. *Journal of Chemistry Materials*, *14*, 1616–1622.

Madieh, S., Simone, M., Wilson, W., Mehra, D., & Augsburger, L. (2007). Investigation of drug–porous adsorbent interactions in drug mixtures with selected porous adsorbents. *Journal of Pharmaceutical Sciences*, *96*, 851–863.

Mura, P., Zerrouk, N., Mennini, N., Maestrelli, F., & Chemtob, C. (2003). Development and characterization of naproxen–chitosan solid systems with improved drug dissolution properties. *European Journal of Pharmaceutical Science*, *19*, 67–75.

Mutalik, S., Anju, P., Manoj, K., & Usha, A. N. (2008). Enhancement of dissolution rate and bioavailability of aceclofenac: A chitosan-based solvent change approach. *International Journal of Pharmaceutics*, *350*, 279–290.

Muzzarelli, R. A. A. (2009). Chitins and chitosans for the repair of wounded skin, nerve, cartilage and bone. *Carbohydrate Polymers*, *76*, 167–182.

Papadimitriou, S., Papageorgiou, G. Z., Kanaze, F. I., Georgarakis, M., & Bikiaris, D. N. (2009). Nanoencapsulation of nimodipine in novel biocompatible poly (propylene-co-butylene succinate) aliphatic copolyesters for sustained release. *Journal of Nanomaterials*, 11. Article ID: 716242.

Park, S. B., You, J. O., Park, H. Y., Haam, S. J., & Kim, W. S. (2001). A novel pH-sensitive membrane from chitosan – TEOS IPN; preparation and its drug permeation characteristics. *Biomaterials*, *22*, 323–330.

Peniche-Covas, C., Argüelles-Monal, W., & San Román, J. (1993). A kinetic study of the thermal degradation of chitosan and a mercaptan derivative of chitosan. *Polymer Degradation and Stability*, *39*, 21–28.

Popat, A., Liu, J., Lu, G. M., & Qiao, S. (2012). PH-responsive drug delivery system based on chitosan coated mesoporous silica nanoparticles. *Journal of Chemistry Materials*, *22*, 11173–11178.

Rashidova, S. S., Shakarova, D. S., Ruzimuradov, O., Satubaldieva, D., Zalyalieva, S., Shpigun, O., et al. (2004). Bionanocompositional chitosan–silica sorbent for liquid chromatography. *Journal of Chromatography B*, *800*, 49–53.

Rinaudo, M. (2006). Chitin and chitosan: Properties and applications. *Progress in Polymer Science*, *31*, 603–632.

Santos, D., Neto, C., Fonseca, J., & Pereira, M. (2008). Chitosan macroporous asymmetric membranes – Preparation, characterization and transport of drugs. *Journal of Membrane Science*, *325*, 362–370.

Soppimath, K. S., Kulkarni, A. R., & Aminabhavi, T. M. (2001). Chemically modified polyacrylamide-g-guar gum-based crosslinked anionic microgels as pH-sensitive drug delivery systems: Preparation and characterization. *Journal of Controlled Release*, *75*, 331–345.

Su, F., Zhao, X., Wang, Y., Zeng, J., Zhou, Z., & Lee, J. (2005). Synthesis of graphitic ordered macroporous carbon with a three-dimensional interconnected pore structure for electrochemical applications. *The journal of Chemistry B*, *109*, 20200–20206.

Tang, X. C., Pikal, M. J., & Taylor, L. S. (2002). A spectroscopic investigation of hydrogen bond patterns in crystalline and amorphous phases in dihydropyridine calcium channel blockers. *Pharmaceutical Research*, *19*, 477–483.

Thanoo, B. C., Sunny, M., & Jayakrishnan, A. (1992). Cross-linked chitosan microspheres: Preparation and evaluation as a matrix for the controlled release of pharmaceuticals. *Journal of Pharmacy and Pharmacology*, *44*, 283–286.

Wu, C., Wang, Z., Zhi, Z., Jiang, T., Zhang, J., & Wang, S. (2011). Development of biodegradable porous starch foam for improving oral delivery of poorly water soluble drugs. *International Journal of Pharmaceutics*, *403*, 162–169.

Chang, X., Chen, D., & Jiao, X. (2008). Chitosan-based aerogels with high adsorption performance. *The Journal of Physical Chemistry B*, *112*, 7721–7725.

Xia, Y., Gates, B., Yin, Y., & Lu, Y. (2000). Monodispersed colloidal spheres: Old materials with new applications. *Advanced Materials*, *12*, 693–713.

Zakhidov, A. A., Baughman, R. H., Iqbal, Z., Cui, C., Khayrullin, I., Dantas, S. O., et al. (1998). Carbon structures with three-dimensional periodicity at optical wavelengths. *Science*, *282*, 897–901.

Zhang, J., Jin, Y., Li, C., Shen, Y., Han, L., Hu, Z., et al. (2009). Creation of three-dimensionally ordered macroporous Au/CeO catalysts with controlled pore sizes and their enhanced catalytic performance for formaldehyde oxidation. *Applied Catalysis B: Environmental*, *91*, 11–20.

Zhao, Q., Wang, T., Wang, J., Zheng, L., Jiang, T., Cheng, G., et al. (2011). Template-directed hydrothermal synthesis of hydroxyapatite as a drug delivery system for the poorly water-soluble drug carvedilol. *Applied Surface Science*, *257*, 10126–10133.

Zheng, X., Yang, R., Tang, X., & Zheng, L. (2007). Part I: Characterization of solid dispersions of nimodipine prepared by hot-melt extrusion. *Drug Development and Industrial Pharmacy*, *33*, 791–802.

Zhu, Y., Cao, H., Tang, L., Yang, X., & Li, C. (2009). Immobilization of horseradish peroxidase in three-dimensional macroporous TiO_2 matrices for biosensor applications. *Electrochimica Acta*, *54*, 2823–2827.